

CrystEngComm

Accepted Manuscript



This is an *Accepted Manuscript*, which has been through the Royal Society of Chemistry peer review process and has been accepted for publication.

Accepted Manuscripts are published online shortly after acceptance, before technical editing, formatting and proof reading. Using this free service, authors can make their results available to the community, in citable form, before we publish the edited article. We will replace this *Accepted Manuscript* with the edited and formatted *Advance Article* as soon as it is available.

You can find more information about *Accepted Manuscripts* in the [Information for Authors](#).

Please note that technical editing may introduce minor changes to the text and/or graphics, which may alter content. The journal's standard [Terms & Conditions](#) and the [Ethical guidelines](#) still apply. In no event shall the Royal Society of Chemistry be held responsible for any errors or omissions in this *Accepted Manuscript* or any consequences arising from the use of any information it contains.

Cite this: DOI: 10.1039/coxx00000x

www.rsc.org/xxxxxx

ARTICLE TYPE

Preparation of $\text{Gd}_2\text{O}_2\text{S}:\text{Er}^{3+},\text{Yb}^{3+}$ phosphor and its multi-wavelength sensitive upconversion luminescence mechanism

Wei Fan,^{a,b} Xiyan Zhang,^c Lixin Chen^c and Liping Lu^{*c}

Received (in XXX, XXX) Xth XXXXXXXXX 20XX, Accepted Xth XXXXXXXXX 20XX

DOI: 10.1039/b000000x

Er^{3+} - Yb^{3+} codoped $\text{Gd}_2\text{O}_2\text{S}$ infrared upconversion phosphor has been prepared via the coprecipitation-solid state reaction process. The composition ratio and calcining conditions have been optimized with orthogonal experiments. X-ray diffraction (XRD) and structure refinement were utilized to analyze the phase composition and the changes of cell parameters. Intense characteristic emissions of Er^{3+} ions were observed when excited by CW laser radiation at 980nm, 1064nm and 1550nm, respectively, which shows that the obtained samples possess the outstanding advantage of application generality in the infrared detection field. The upconversion luminescence mechanisms excited at different wavelengths were discussed by means of the Intensity-Power test.

1. Introduction

Up-conversion materials have many interesting applications, such as upconversion lasers,¹⁻² infrared quantum counters,³ adsorbents for coloured effluents,⁴ fluorescence bioimaging agents⁵⁻⁷, laser lighting or displays,⁸ solar cells,⁹⁻¹⁰ et al. A large number of 980nm upconversion materials have been studied systematically,¹¹⁻¹³ for example, Takayuki Hirai group¹⁴ and Timur Sh Atabaev group¹⁵ prepared $\text{Gd}_2\text{O}_3:\text{Yb}$, Er phosphors using the emulsion liquid method and urea homogeneous precipitation method, respectively, and they measured the upconversion emissions under the excitation of 980nm-990nm and studied the two-photon absorption luminescence mechanism, aiming at luminescent reporter in the field of bioluminescence. However, only a few 1064nm and 1550nm upconversion materials were reported, for example, Jianguo Deng¹⁶ reported that the dopant of La^{3+} would promote the upconversion luminescence of $\text{TiO}_2:\text{Er}$, Yb excited at 1064nm; Vermelho¹⁷ and RI Su-Hyon¹⁸ studied respectively the upconversion emissions of Er -doped tellurite glasses and $\text{Y}_2\text{O}_2\text{S}:\text{Er}^{3+}$, Yb^{3+} phosphor, when excited at 1540-1550nm.

In view of 980nm, 1064nm and 1550nm are the popular working wavelengths in the near-infrared band, both the study of luminescence properties and the study of physical mechanism of the multi-wavelength sensitive upconversion materials are important to multi-wavelength infrared detection. Oxysulfide upconversion phosphors possess the outstanding advantages of low phonon energy, high upconversion efficiency and excellent stability; therefore they have attracted so much attention in the past 10 years.¹⁹ Herein, we synthesized the Er^{3+} - Yb^{3+} co-doped gadolinium oxysulfide phosphor by the coprecipitation-solid state reaction process and will discuss its multi-wavelength sensitive upconversion luminescence.

2. Experimental

Preparation

$\text{Gd}_2\text{O}_2\text{S}:\text{Er}^{3+},\text{Yb}^{3+}$ upconversion phosphors were synthesized through the Coprecipitation-Solid state reaction method. The purity of the rare earth oxide starting material erbium oxide (Er_2O_3), ytterbium oxide (Yb_2O_3), and gadolinium oxide (Gd_2O_3) was 99.999% and that of sodium carbonate (Na_2CO_3), oxalic acid ($\text{C}_2\text{H}_2\text{O}_4$) and sulfur (S) was analytical grade. The oxide precursor was synthesized by the coprecipitation process, and the procedure was as follows: Gd_2O_3 , Er_2O_3 and Yb_2O_3 were dissolved in $8\text{mol}\cdot\text{L}^{-1}$ nitric acid to obtain the rare earth nitrate solution mixture, and then the $0.5\text{mol}\cdot\text{L}^{-1}$ oxalate solution was dropped into the solution mixture until it was precipitated completely (adjusting $\text{pH}=5$). After 5-6 hours' standing, suction filtrating, washing by water and absolute ethyl alcohol, and drying in an 80°C oven, the ultrafine rare earth oxide precursor was obtained, and it was calcined sequentially.

Orthogonal experiments were carried out in order to optimize the calcining technological parameters. An orthogonal standard table $L_{16}(4^4)$ was adopted, and the experiments were carried out in accordance with the layouts of the orthogonal array (wherein Er to Yb concentration ratio is one to five). S and Na_2CO_3 were added into the above rare earth oxide precursor to be ground thoroughly, then this mixture was put into a muffle to calcine, in a mild reducing atmosphere, at a certain temperature for a certain length of time to get the $\text{Gd}_2\text{O}_2\text{S}:\text{Er}^{3+},\text{Yb}^{3+}$ phosphor.

Measurements

The X-ray diffraction (XRD) patterns were performed on a Rigaku D/max 2500 PC diffractometer at a step of 0.02° with a standing time of 2s/step in the 2θ range from 10° to 120° , and $\text{Cu K}\alpha_1$ ($\lambda=0.15406\text{nm}$) worked as a radiation source, with an accelerating voltage of 20 kV and a working current of 10 mA. The structure refinement was done using the General Structure Analysis System (GSAS) program. A SHIMADZU RF-5301PC fluorescence spectrometer coupled respectively with different

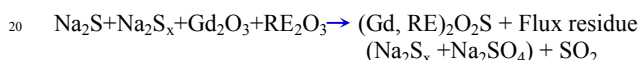
excitation sources of 980nm, 1064nm and 1550nm laser was utilized to test the IR up-conversion spectra of the samples, and the Intensity-Power curves were tested with the help of a series of optical attenuators.

3. Results and discussion

Optimization of the calcining parameters by using the orthogonal experiments

It is well known that the upconversion luminescence intensity and the red/green emission ratio are closely related to the Er^{3+} doping concentration and $\text{Yb}^{3+}/\text{Er}^{3+}$ concentration ratio, especially at the excitation of 1550nm. Considering application generality (980nm, 1064nm and 1550nm), $\text{Yb}^{3+}/\text{Er}^{3+}$ concentration ratio was set 5:1. The general formula of the sample can be represented as $(\text{Gd}_{1-6x}\text{Er}_x\text{Yb}_{5x})_2\text{O}_2\text{S}$.

Na_2CO_3 was adopted as fluxing agent. It can react with S to form intermediate products to promote the synthesis reaction, improving the structural integrity of the product lattice. and the reaction equations are as follows:²⁰



Experiments were carried out in accordance with the layouts of the $L_{16}(4^4)$ orthogonal array and then all of the spectra of samples excited at different wavelengths were tested (shown in Fig. 1-3). The excitation source of SHIMADZU RF-5301PC fluorescence spectrometer was replaced with an infrared laser, which was led into by the optical fiber. It would be noticed that the head of optical fiber should be fixed in the same position in each test in order to guarantee the same excitation power density, which was $1.6\text{W}/\text{cm}^2$ for 980nm, $160\text{mW}/\text{cm}^2$ for 1064nm and $180\text{mW}/\text{cm}^2$ for 1550nm. The equal mass powder was pressed under the same condition to form thin sheets in order to decrease the effect of diffuse scattering of powder particles.

It can be seen that all the spectra exhibit the characteristic emission peaks of Er^{3+} ions. The orthogonal analysis results were listed in **Table 1**, with the sum of the red and green emission intensity excited at different wavelength as the evaluation index (shown as the ratio of the intensity of each sample to the intensity of optimal sample in Table 1). k_1^- , k_2^- , k_3^- and k_4^- are the mean of the corresponding intensity. It can be found from Table 1 that the optimum condition resulting from different wavelength orthogonal analysis is inconsistent, for example, it is $A_4 B_3 C_1 D_2$ for the excitation of 980nm; it is $A_3 B_3 C_1 D_2$ for the excitation of 1064nm and it is $A_2 B_4 C_2 D_4$ for the excitation of 1550nm. By contrast, the upconversion luminescence intensity excited at 980nm and 1550nm is stronger than that excited at 1064nm, therefore, the determination of the optimum condition should take the specific application requirements into account. If the dominant green emissions are considered, the ideal conditions should coincide with the optimal conditions determined by orthogonal analysis, which can be known from the green/red ratio of the samples (shown in Table 2). Take 980nm excitation for example, the green/red ratio of the No.11 sample and No.16 sample is 12 and 14, respectively, while the ratio of other sample is 17~20. However, not only the green/red ratio but also the

intensity value should be taken into consideration.

In view of 980nm, 1064nm and 1550nm are the popular working wavelengths in the near-infrared band. If all of the above three infrared wavelengths are considered, the ideal conditions can be chosen as $A_3 B_3 C_2 D_2$ (1050°C , 3.0h, Er^{3+} concentration 2%, Yb^{3+} concentration 10%, $m_{(\text{Gd}_2\text{O}_3)} : m_{(\text{S})} : m_{(\text{Na}_2\text{CO}_3)} = 10:4.5:3.5$), then, this determined condition was adopted to prepare the sample in order to test and analyze its structure and properties, and its formula can be represented as $^{65}(\text{Gd}_{0.88}\text{Er}_{0.02}\text{Yb}_{0.1})_2\text{O}_2\text{S}$.

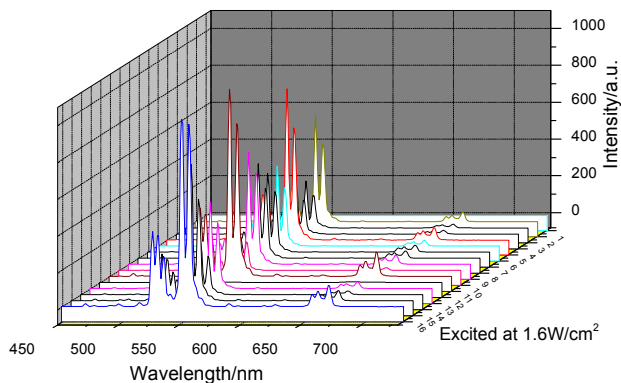
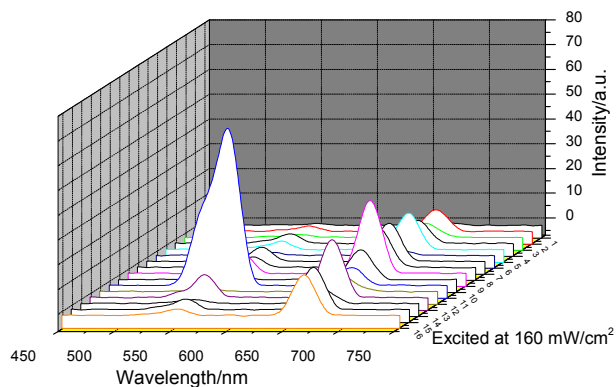
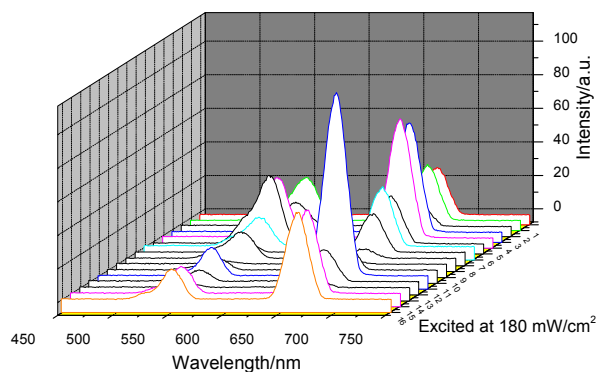
Tab.1 Experimental layouts and results of orthogonal experiments $L_{16}(4^4)$

Trial No.	A	B	C	D	Intensity ratio of each I to maximum I Excited at 980nm	Intensity ratio of each I to maximum I Excited at 1064nm	Intensity ratio of each I to maximum I Excited at 1550nm
	Calcining temperature	Calcining time	$n(\text{Er}^{3+})$	$m_{(\text{Gd}_2\text{O}_3)}:m_{(\text{S})}:m_{(\text{Na}_2\text{CO}_3)}$			
1	950°C	2.0 h	1.5%	10: 4.5: 3.2	0.3%	0.03%	26%
2	950°C	2.5 h	2%	10: 4.5: 3.5	54%	10.5%	44%
3	950°C	3.0 h	2.5%	10: 4.5: 3.8	24%	6%	20%
4	950°C	3.5 h	3%	10: 4.5: 4.0	23%	14%	60%
5	1000°C	2.0 h	2%	10: 4.5: 3.8	75%	21%	82%
6	1000°C	2.5 h	1.5%	10: 4.5: 4.0	40%	1.2%	52%
7	1000°C	3.0 h	3%	10: 4.5: 3.2	37%	26%	43%
8	1000°C	3.5 h	2.5%	10: 4.5: 3.5	47%	24%	23%
9	1050°C	2.0 h	2.5%	10: 4.5: 4.0	52%	49%	17%
10	1050°C	2.5 h	3%	10: 4.5: 3.8	20%	20%	3%
11	1050°C	3.0 h	1.5%	10: 4.5: 3.5	100%	100%	23%
12	1050°C	3.5 h	2%	10: 4.5: 3.2	0.4%	11%	100%
13	1100°C	2.0 h	3%	10: 4.5: 3.5	43%	43%	20%
14	1100°C	2.5 h	2.5%	10: 4.5: 3.2	26%	6.6%	5.5%
15	1100°C	3.0 h	2%	10: 4.5: 4.0	68%	27%	52%
16	1100°C	3.5 h	1.5%	10: 4.5: 3.8	98%	23%	55%
k_1^-	25%	43%	59%	16%	orthogonal analysis result excited at 980nm		
k_2^-	49%	35%	49%	61%			
k_3^-	43%	57%	37%	54%			
k_4^-	58%	42%	30%	45%			
k_1^-	7.6%	28%	31%	10%	orthogonal analysis result excited at 1064nm		
k_2^-	18%	9.5%	17%	44%			
k_3^-	45%	39%	21%	17%			
k_4^-	25%	18%	25%	22%			
k_1^-	37%	36%	39%	43%	orthogonal analysis result excited at 1550nm		
k_2^-	50%	26%	69%	27%			
k_3^-	35%	34%	16%	40%			
k_4^-	33%	59%	31%	45%			

Take into consideration the multi-wavelength application, the ideal conditions are as follows: $A_3 B_3 C_2 D_2$ (1050°C , 3.0h, Er^{3+} concentration is 2%, corresponding Yb^{3+} concentration is 10%, the amount of fluxing agent is as follows : $m(\text{Gd}_2\text{O}_3):m(\text{S}):m(\text{Na}_2\text{CO}_3)=10:4.5:3.5$)

Tab.2 Green/red ratio of the $L_{16}(4^4)$ orthogonal samples

Trial No.	Green/red ratio Excited at 980nm	Green/red ratio Excited at 1064nm	Green/red ratio Excited at 1550nm	Trial No.	Green/red ratio Excited at 980nm	Green/red ratio Excited at 1064nm	Green/red ratio Excited at 1550nm
1	0.8	0.15	0.25	9	16	0.20	3.1
2	17	0.18	0.77	10	20	0.30	0.5
3	18	0.17	0.95	11	12	12	0.33
4	19	0.25	0.19	12	0.5	0.17	0.15
5	17	0.13	0.49	13	20	0.3	0.36
6	20	0.30	1.5	14	18	0.16	0.5
7	19	0.17	0.48	15	21	0.16	0.3
8	17	0.17	0.21	16	14	0.15	0.35

Fig.1 Upconversion spectra of $L_{16}(4^4)$ orthogonal samples at the excitation of 980nmFig.2 Upconversion spectra of $L_{16}(4^4)$ orthogonal samples at the excitation of 1064nmFig.3 Upconversion spectra of $L_{16}(4^4)$ orthogonal samples at the excitation of 1550nm

Phase identification and crystal structure

The XRD pattern of $(\text{Gd}_{0.88}\text{Er}_{0.02}\text{Yb}_{0.1})_2\text{O}_2\text{S}$ sample is shown in Fig.4 in comparison with the standard peak positions of the $\text{Gd}_2\text{O}_2\text{S}$ hexagonal phase (JCPDS card No. 26-1422). The XRD results show that the solid solution is formed and the sample is in a hexagonal $\text{Gd}_2\text{O}_2\text{S}$ structure with the space group of $P-3m1(164)$. The Er^{3+} and Yb^{3+} ions are expected to efficiently dissolve in the $\text{Gd}_2\text{O}_2\text{S}$ host lattice by replacing the Gd^{3+} sites; thus, no other phase or impurity phase can be detected.

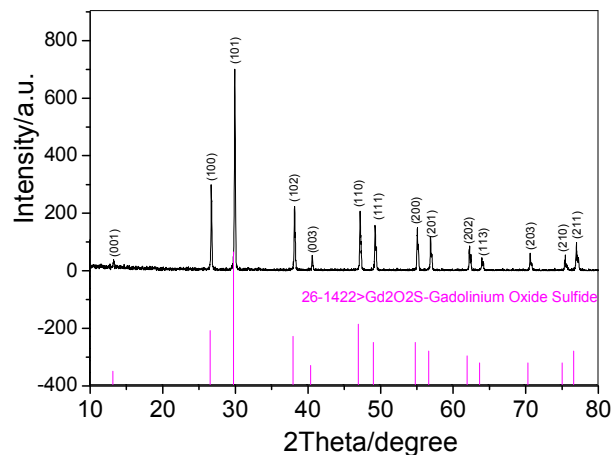
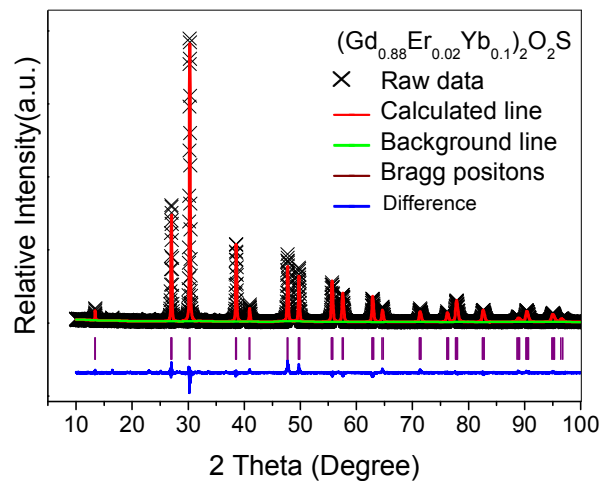
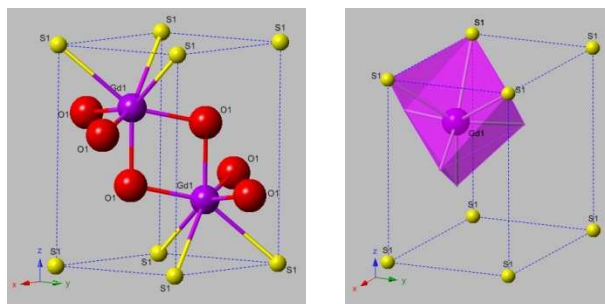
Fig.4 XRD pattern of $(\text{Gd}_{0.88}\text{Er}_{0.02}\text{Yb}_{0.1})_2\text{O}_2\text{S}$ sampleFig.5 Experimental (cross), calculated (solid line), and difference (bottom blue line) results of XRD refinements of $(\text{Gd}_{0.88}\text{Er}_{0.02}\text{Yb}_{0.1})_2\text{O}_2\text{S}$ (a) Coordination of Gd^{3+} ions (b) Gd-O-S coordination polyhedronFig.6 Crystal structure representation of $\text{Gd}_2\text{O}_2\text{S}$

Fig.5 shows the observed, calculated, and difference patterns of the $(\text{Gd}_{0.88}\text{Er}_{0.02}\text{Yb}_{0.1})_2\text{O}_2\text{S}$ phosphor. The final refinement converged with weighted profiles of $\chi^2 = 1.84$, $R_p = 9.77\%$ and $R_{wp} = 13.03\%$, thus revealing the good quality of the refinement. Fig.6 is the crystal structure of $\text{Gd}_2\text{O}_2\text{S}$. There is only one coordination type of Gd^{3+} , and each metal atom Gd seems to be bonded to four oxygen atoms and three sulfur atoms to form a seven coordination polyhedron.

It can be seen from the XRD patterns that the diffraction peaks have shifted right slightly in comparison with the peak positions of the standard card (No. 26-1422). It is because that the difference of ionic radius between Er^{3+} (0.0881nm) / Yb^{3+} (0.0858nm) and Gd^{3+} (0.0938nm) results in the unit cell shrinkage. Considering that $\text{Gd}_2\text{O}_2\text{S}$ is of hexagonal structure, the interplanar crystal spacing d can be calculated as following equation:

$$d = \frac{1}{\sqrt{\frac{4}{3a^2}(h^2 + k^2 + hk) + \frac{l^2}{c^2}}} \quad (\text{Equation 1})$$

The unit cell shrinkage will cause the decrease of d , and the consequent right shift of those diffraction peaks. The original cell parameters of $\text{Gd}_2\text{O}_2\text{S}$ are $3.852\text{\AA} \times 3.852\text{\AA} \times 6.667\text{\AA} <90^\circ \times 90^\circ \times 120^\circ>$, while the cell parameters of $(\text{Gd}_{0.88}\text{Er}_{0.02}\text{Yb}_{0.1})_2\text{O}_2\text{S}$ are $a = b = 3.813\text{\AA}$, $c = 6.616\text{\AA}$, $\alpha = \beta = 90^\circ$ and $\gamma = 120^\circ$, which are calculated from the above refinement of XRD pattern.

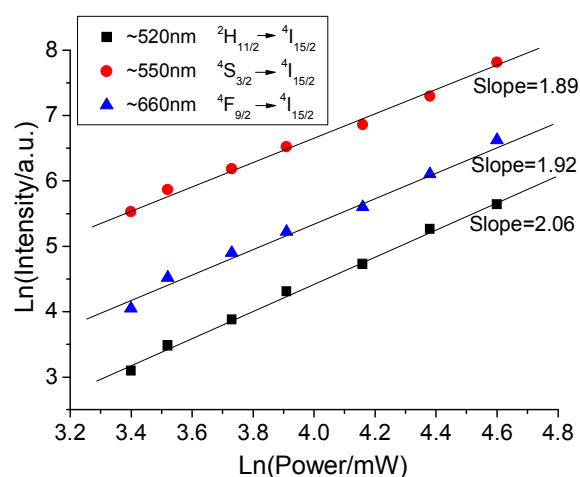
Luminescence mechanism analysis

Experiments have proved that the emission spectrum of the trivalent rare earth doped upconversion material will change along with the matrix categories and excitation power.²¹ It is known that for unsaturated upconversion processes, the number of photons which are required to populate the upper emitting state can be obtained by the following relation:²²

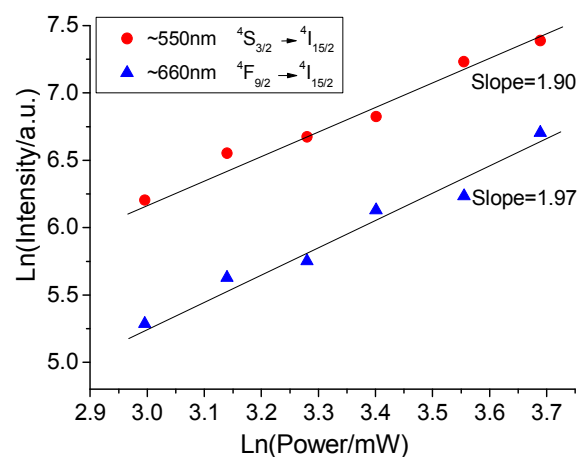
$$I_{\text{vis}} = P_{\text{NIR}}^n \quad (\text{Equation 2})$$

Where I_{vis} is the fluorescence intensity, P_{NIR} is the pump laser power, and n is the number of pump-photons required to populate the emitting state.

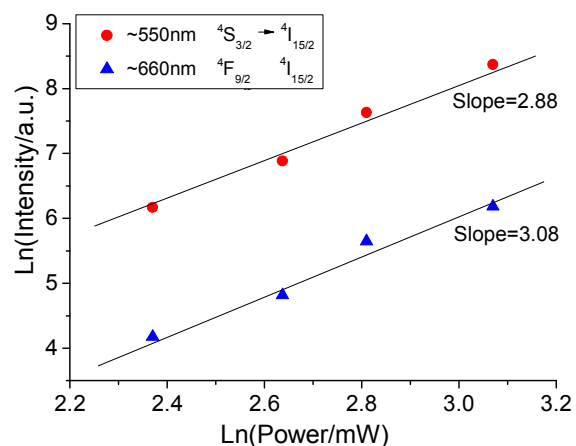
Fig.7 (a) shows the measured power dependence of the three upconversion emissions of Er^{3+} ions excited at 980nm at room temperature for the $(\text{Gd}_{0.88}\text{Er}_{0.02}\text{Yb}_{0.1})_2\text{O}_2\text{S}$ sample. The results are illustrated in the \ln - \ln plots, and the values of slopes for the $\sim 520\text{nm}$ green emission, $\sim 550\text{nm}$ green emission and $\sim 660\text{nm}$ red emission are 2.06, 1.89 and 1.92, respectively. The results indicate that two-photon process is mainly responsible for the observed up-converted emission for the excitation of 980nm. The dependences excited at 1064nm and 1550nm are illustrated in the \ln - \ln plots of Fig.7 (b) and Fig.7 (c). The green and red emissions exhibit a sub-square (1.90 and 1.97) power-law behavior for the excitation of 1064nm and a sub-cubic (2.88 and 3.08) power-law behavior for the excitation of 1550nm, which indicates that two pumping photons around 1064nm and three pumping photons around 1550nm participate in the upconversion excitation process, respectively.



(a) Excited at 980nm



(b) Excited at 1064nm



(c) Excited at 1550nm

Fig.7 \ln - \ln plots of the green and red emission versus excitation power

(a) Excited at 980nm (b) Excited at 1064nm (c) Excited at 1550nm

Fig.8 shows the simplified Yb³⁺-Er³⁺ energy-level diagram of the 980nm upconversion luminescence of the sample. It has been known from the above I-P curves that all of the 520nm, 550nm and 660nm emissions originate from two-photon absorption process. First, the electrons can be pumped from the Er³⁺ ground state ⁴I_{15/2} to its excited ⁴I_{13/2} level, through the direct absorption of Er³⁺ ions or the energy transfer between Yb³⁺ and Er³⁺ ions. The energy difference between ²F_{5/2} and ²F_{7/2} level of Yb³⁺ ions and the energy difference between ⁴I_{15/2} and ⁴I_{13/2} level of Er³⁺ ions are approximately equal to 10300cm⁻¹, and also the absorption cross section of Yb³⁺ is greatly larger than that of Er³⁺, therefore the population of ⁴I_{13/2}(Er³⁺) level is mainly realized by Yb³⁺-Er³⁺ energy transfer process (ETU). Similarly, Er³⁺ ions can be promoted from the ⁴I_{13/2} level to the ⁴F_{9/2} level through another ETU process, that is ²F_{5/2}(Yb³⁺) + ⁴I_{13/2}(Er³⁺) → ²F_{7/2}(Yb³⁺) + ⁴F_{9/2}(Er³⁺) (②). Er³⁺ ions at the ⁴F_{9/2} level might relax to the ²H_{11/2} and ⁴S_{3/2} levels by fast multiphonon process. Then, the radiative decay from the ²H_{11/2} and ⁴S_{3/2} level to the ground state ⁴I_{15/2} generates green UC luminescence around 520nm and 550nm, respectively.

Red UC luminescence at the excitation of 980 nm results from ⁴F_{9/2}→⁴I_{15/2} transitions. The population mechanism of ⁴F_{9/2} level is relatively complicated, and it includes nonradiative relaxation and cross relaxation processes.^{18, 24} Er³⁺ ions at the ⁴S_{3/2} level possibly occur the non-radiative relaxation process to reach the ⁴F_{9/2} level, or Er³⁺ ions at the ⁴I_{11/2} level can firstly relax nonradiatively to the next lower ⁴I_{13/2} level and then transit to the ⁴F_{9/2} level through Er³⁺-Yb³⁺ energy-transfer process(③). In addition, the ⁴F_{9/2} state can also be populated via the ⁴F_{7/2}(Er³⁺)+⁴I_{11/2}(Er³⁺)→ 2 ⁴F_{9/2}(Er³⁺) (④) cross relaxation process.

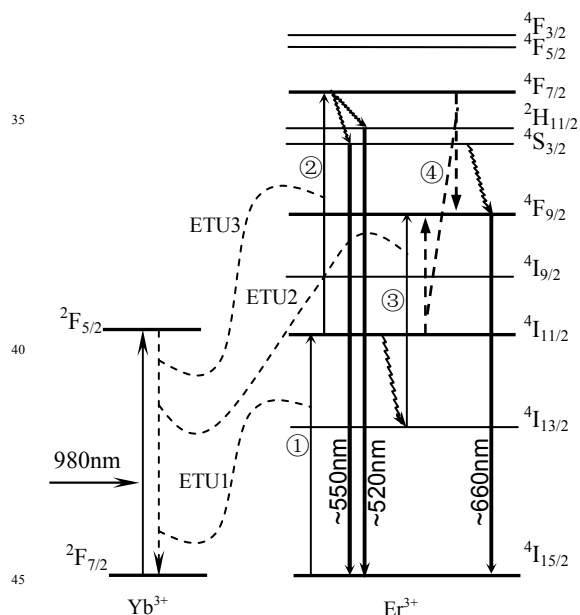


Fig.8. Er³⁺-Yb³⁺ energy level diagram with the proposed UC mechanisms excited at 980nm

Fig.9 shows the simplified Yb³⁺-Er³⁺ energy-level diagram of the 1064nm upconversion luminescence of the sample. The green

and red emissions of Er³⁺ ions result from two-photon absorption process (shown as Fig.7 (b)). Er³⁺ ions at the ⁴I_{15/2} level can absorb directly 1064 nm infrared light to transit to ⁴I_{13/2} level, and it can be seen from the Gd₂O₃: Er, Yb absorption spectrum reported by Ajithkumar¹⁰ that 1064 nm light can also be absorbed partially by Yb³⁺ ions, therefore the population mechanism of ⁴I_{13/2}(Er³⁺) level includes both the Er³⁺ ground state absorption (GSA) process and the Yb³⁺-Er³⁺ energy-transfer upconversion (ETU) process. Once in the ⁴I_{13/2} level, the following energy-transfer, nonradiative relaxation and cross relaxation processes are similar to that of 980 nm excitation.

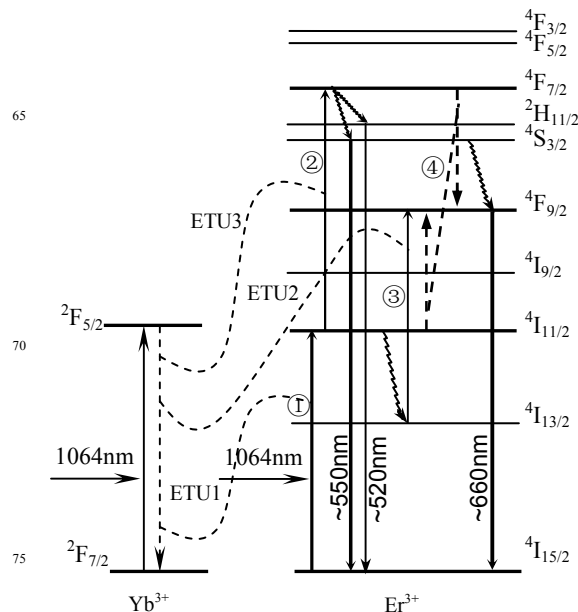


Fig.9. Er³⁺-Yb³⁺ energy level diagram with the proposed UC mechanisms excited at 1064nm

Fig.10 presents the energy-level diagram of the 1550nm upconversion luminescence of the sample. The green and red emissions of Er³⁺ ions result from three-photon absorption process (shown as Fig.7 (c)). Yb³⁺ ions cannot absorb 1550 nm infrared light, while Er³⁺ ⁴I_{15/2}→⁴I_{13/2} transitions can match up with the energy of 1550 nm, hence the UC luminescence should depend on the Er³⁺ absorption process and Er³⁺-Er³⁺ energy-transfer process. When excited by 1550nm infrared light, Er³⁺ ions are promoted from the ground state ⁴I_{15/2} to the first excited state ⁴I_{13/2} (①). Population of higher Er³⁺ excited states can be realized by excited state absorption (ESA) process and/or ETU process. As far as high Er³⁺ dopant concentration is concerned, the ETU process is dominant, that is ⁴I_{13/2}(Er³⁺) + ⁴I_{13/2}(Er³⁺) → ⁴I_{15/2}(Er³⁺) + ⁴I_{9/2}(Er³⁺) (②).²⁵⁻²⁶ Similarly, Er³⁺ ions can be promoted from the ⁴I_{9/2} state to the ²H_{11/2} state through ETU process, that is ⁴I_{9/2}(Er³⁺) + ⁴I_{13/2}(Er³⁺) → ²H_{11/2}(Er³⁺) + ⁴I_{15/2}(Er³⁺) (③). Er³⁺ ions at the ²H_{11/2} state might relax to the ⁴S_{3/2} level by fast multiphonon process. Then, the radiative decay from the ²H_{11/2} and ⁴S_{3/2} state to the ground state generates green UC luminescence around 520nm and 550nm, respectively. Er³⁺ ions at the ⁴S_{3/2} state might relax non-radiatively to the ⁴F_{9/2} state. Furthermore, as far as those Er³⁺ ions promoted to the excited state ⁴I_{9/2} are concerned, considering the short lifetime of the ⁴I_{9/2}

state (around 16 μ s) and the small energy gap between $^4I_{9/2}$ and $^4I_{11/2}$ levels (around 2000 cm^{-1}), it is clear that fast multiphonon relaxation to the $^4I_{11/2}$ level occurs. After the population of the $^4I_{11/2}$ level, the $^4F_{9/2}$ emitting state is populated via the $^4I_{11/2}(\text{Er}^{3+}) + ^4I_{13/2}(\text{Er}^{3+}) \rightarrow ^4F_{9/2}(\text{Er}^{3+}) + ^4I_{15/2}(\text{Er}^{3+})$ ETU process giving rise to red UC emission bands centered at $\sim 660\text{nm}$.¹⁷

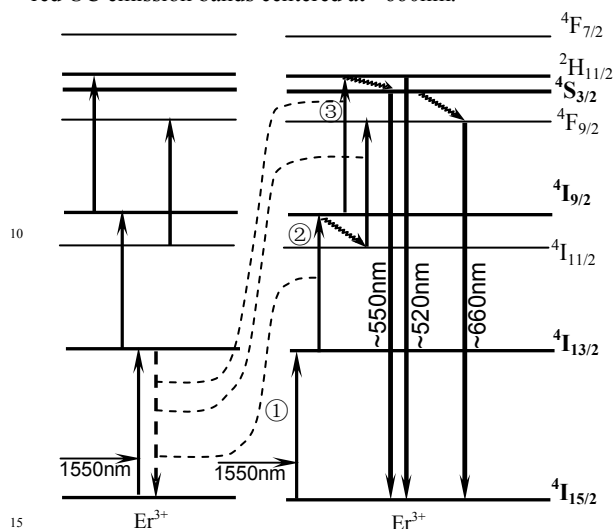


Fig.10. Er^{3+} energy level diagram with the proposed UC mechanisms excited at 1550nm

20 Spectral analysis

Ajithkumar and his group tested UV-Vis-NIR absorption spectrum of $\text{Gd}_2\text{O}_3\text{:Er, Yb}$ sample as shown in Fig.11.¹⁰ From their measured result, it can be seen that there are the absorption bands of Yb^{3+} ion corresponding to $^2F_{7/2} \rightarrow ^2F_{5/2}$ transitions in the 900-1100nm range and the absorption bands of Er^{3+} ion corresponding to $^4I_{15/2} \rightarrow ^4I_{13/2}$ transitions around 1500nm.

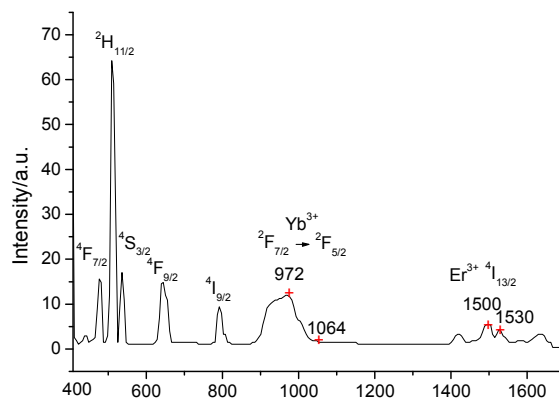
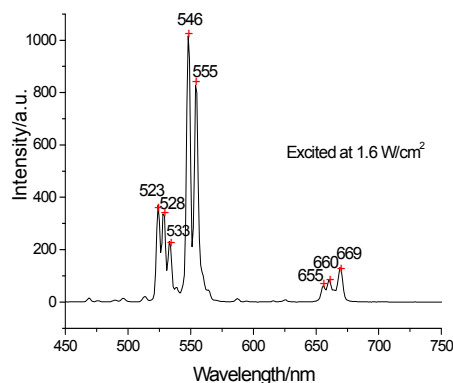


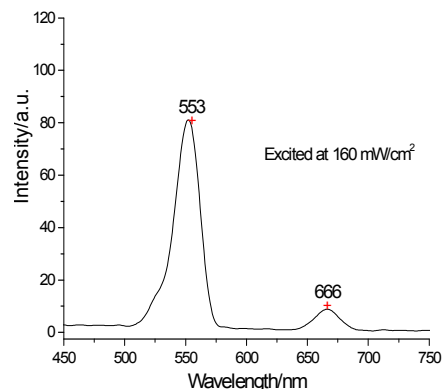
Fig.11 UV-Vis-NIR absorption spectrum of $\text{Gd}_2\text{O}_3\text{:Er, Yb}$

Fig.12 shows a series of upconversion spectra excited at various wavelengths. All three spectra exhibit the Er^{3+} characteristic green and red emissions. The emission peaks at ~ 520 , $\sim 550\text{nm}$ and $\sim 660\text{nm}$ correspond to the $^2H_{11/2} \rightarrow ^4I_{15/2}$, $^4S_{3/2} \rightarrow ^4I_{15/2}$ and $^4F_{9/2} \rightarrow ^4I_{15/2}$ transitions, respectively. The emission spectra excited at 980nm and 1064nm are characterized

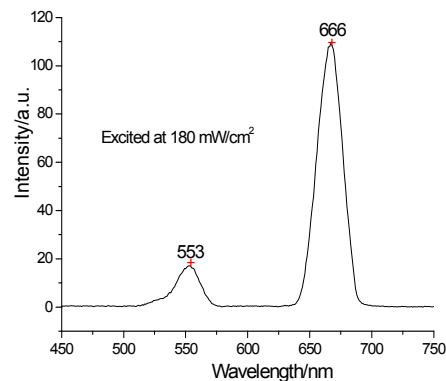
by an intense green band followed by a weaker red band, while the emission spectrum excited at 1550nm presents an intense red band. The $^4I_{15/2} \rightarrow ^4I_{13/2}$ transitions of Er^{3+} ions match the energy of 1550 nm infrared light very well, therefore the $^4I_{13/2}$ level is populated easily, and subsequently $^4I_{9/2}$ level is populated through ETU and/or ESA process. The Er^{3+} ions at $^4I_{9/2}$ level would be likely to transit nonradiatively to $^4I_{11/2}$ level because of the short lifetime of $^4I_{9/2}$ level, and then followed by the $^4I_{11/2} \rightarrow ^4F_{9/2}$ transitions through ETU process. In conclusion, the population of $^4F_{9/2}$ level at the excitation of 1550 nm is higher apparently than that at the excitation of 980 nm and 1064 nm, and then the Er^{3+} red emission at $\sim 660\text{nm}$ resulting from $^4F_{9/2} \rightarrow ^4I_{15/2}$ transitions becomes stronger.



(a) excited at 980nm



(b) excited at 1064nm



(c) excited at 1550nm

Fig.12 Upconversion spectra of the optimal sample excited at different wavelengths

The ~520nm emission peaks have not been observed in the spectra excited at 1064nm and 1550nm. Though the $^2H_{11/2}$ level can be populated firstly by the ETU process and the multiphonon relaxation process, energy level depopulation occurs immediately through $^2H_{11/2} \rightarrow ^4S_{3/2}$ non-radiative transition because the band edge of the $S^{2-}-Er^{3+}$ charge transfer state (CTS) is lower than that of the $^2H_{11/2}$ level, which leads to an efficient population of the $^4S_{3/2}$ state, therefore, under the low exciting power, it is a small amount that populated on the $^2H_{11/2}$ level. That is why the $^2H_{11/2} \rightarrow ^4I_{15/2}$ transitions (~520nm emission) have not been observed in the two spectra excited at 1064nm and 1550nm.²⁷⁻²⁸

Furthermore, it can be seen from the spectrum excited at 980nm that there exist split peaks because of the high exciting power. The green emission which is due to the $^2H_{11/2} \rightarrow ^4I_{15/2}$ transitions shows Stark levels at 523, 528 and 533 nm, the ~550 nm emission ($^4S_{3/2} \rightarrow ^4I_{15/2}$) shows Stark levels at 546 and 555nm, and the ~660nm emission ($^4F_{9/2} \rightarrow ^4I_{15/2}$) shows Stark levels at 655, 660 and 669nm.

The number of Stark energy levels splitting can be calculated by group theory.²⁹ In the case of high excitation energy, every single energy level can split in several Stark levels, which can be expressed as a linear combination of irreducible representation. The space group of hexagonal Gd_2O_2S is P-3m1. The total angular momentum quantum number J of Er^{3+} is semi-integer; hence the energy levels splitting can be represented by the character equation of bi-group, then the Er^{3+} ground state $^4I_{15/2}$ can be calculated as:

$$\chi \left[D_{\pm}^{\pm}(R_{\theta}) \right] = \frac{\sin\left(J + \frac{1}{2}\right)\theta}{\sin\left(\frac{\theta}{2}\right)}$$

Where χ is group character, \pm denotes the parity under the inversion operation, R_{θ} is rotation angle along the rotation axis, and J is total angular momentum quantum number. The calculated group characters of Er^{3+} ground state $^4I_{15/2}$ are as follows: $E = 16$, $C_2 = 0$, $C_3 = -1$, $C_4 = 0$, in which $E=2J+1$. Comparing with group-group character table, the linear combination of irreducible representation is:³⁰

$$\Gamma_{(J=15/2)} = 5\Gamma_4 + 2(\Gamma_5 + \Gamma_6)$$

The above combination formula means that Er^{3+} ground state $^4I_{15/2}$ could split in 2 Stark energy levels in this crystal field. Similarly, the linear combinations of irreducible representation of $^2H_{11/2}$, $^4S_{3/2}$ and $^4F_{9/2}$ are:

$$\Gamma_{(J=11/2)} = 4\Gamma_4 + 2(\Gamma_5 + \Gamma_6)$$

$$\Gamma_{(J=3/2)} = \Gamma_4 + (\Gamma_5 + \Gamma_6)$$

$$\Gamma_{(J=9/2)} = 3\Gamma_4 + 2(\Gamma_5 + \Gamma_6)$$

That means all of the excited $^2H_{11/2}$, $^4S_{3/2}$ and $^4F_{9/2}$ levels of Er^{3+} ions could split in 2 Stark energy levels in hexagonal Gd_2O_2S crystal lattice, therefore, up to four transitions of different wavelength can be obtained between each of the above excited level and the ground state. The upconversion spectrum excited at

980 nm (Fig.12(a)) is basically in line with the calculated results.

50 Conclusions

$Er^{3+}-Yb^{3+}$ codoped Gd_2O_2S infrared upconversion phosphor was synthesized via the coprecipitation-solid state reaction process. The ideal synthesis conditions, calcined at 1050°C for 3.0h, with Er^{3+} and Yb^{3+} dopant concentration of 2% and 10% and mass percent of $m_{(Gd_2O_3)}:m_{(S)}:m_{(Na_2CO_3)}=10:4.5:3.5$, were determined through $L_{16}(4^4)$ orthogonal experiments. XRD and structure refinement were utilized to analyze the phase composition and the changes of cell parameters, and the results show that the sample is of hexagonal Gd_2O_2S structure and the cell parameters have changed to $3.813\text{\AA} \times 3.813\text{\AA} \times 6.616\text{\AA} < 90^\circ \times 90^\circ \times 120^\circ >$ from $3.852\text{\AA} \times 3.852\text{\AA} \times 6.667\text{\AA} < 90^\circ \times 90^\circ \times 120^\circ >$. The multi-wavelength sensitive upconversion luminescence mechanisms were studied by means of the ln-ln plots of Intensity-Power (I-P) curve. The result of I-P test shows that the upconversion luminescence under the excitation of 980nm and 1064nm can be attributed to two-photon process, while that of 1550nm can be attributed to three-photon process.

Acknowledgements

This work was supported by the National Natural Science Foundation of China (Grant No.61307118) and Jilin Province Science and Technology Department Project (Grant No. 20130102016JC).

Notes

^a Department of Chemistry, Northeast Normal University, Changchun 130024, Jilin, PR China. E-mail: fanw633@163.com

^b School of Chemical and environmental Engineering, Changchun University of Science and Technology, Changchun 130022, Jilin, PR China. Tel: +86-431-85582542

^c School of Materials Science and Engineering, Changchun University of Science and Technology, Changchun 130022, Jilin, PR China. Tel: +86-431-85583147; *Corresponding E-mail: luliping771219@126.com

References

- [1] L. L. Wang, W. P. Qin, Z. Y. Liu, D. Zhao, G. S. Qin, W. H. Di and C. F. He. *Opt. Express*, 2012, 20, 7602-7607.
- [2] W. Yu, W. Xu, H. W. Song and S. Zhang. *Dalton Trans.*, 2014, 43, 6139-6147
- [3] H. Jia, C. Xu, J. C. Wang, P. Chen, X. F. Liu and J. R. Qiu, *CrystEngComm*, 2014, 16, 4023-4028.
- [4] X. J. Li, Z. Y. Hou, Y. Zhang, G. Zhang, J. S. Lian and J. Lin, *Dalton Trans.*, 2014, 43, 15457-15464.
- [5] L. Wang, J. H. Liu, Y. L. Dai, Q. Yang, Y. X. Zhang, P. P. Yang, Z. Y. Cheng, H. Z. Lian, C. X. Li, Z. Y. Hou, P. A. Ma and J. Lin, *Langmuir*, 2014, 30, 13042-13051
- [6] S. A. Osseni, S. Lechevallier, M. Verelst, P. Perriat, J. Dexpert-Ghys, D. Neumeyer, R. Garcia, F. Mayer, K. Djanashvili, J. A. Peters, E. Magdeleine, H. Gros-Dagnac, P. Celsis and R. Mauricot, *Nanoscale*, 2014, 6, 555-564.
- [7] D. K. Ma, D. P. Yang, J. L. Jiang, P. Cai and S. M. Huang, *CrystEngComm*, 2010, 12, 1650-1658.
- [8] J. Yang, C. M. Zhang, C. Peng, C. X. Li, L. L. Wang, R. T. Chai, J. Lin, *Chem. Eur. J.*, 2009, 15, 4649-4655.
- [9] W. G. van Sark, J. de Wild, J. K. Rath, A. Meijerink and R. E. Schropp, *Nanoscale Res. Lett.*, 2013, 8, 81.
- [10] G. Ajithkumar, Benjamin Yoo, Dara E. Goral, Peter J. Hornsby, Ai-Ling Lin, Uma Ladiwala, Vinayak P. Dravid and Dhiraj K. Sardar, *J. Mater. Chem. B*, 2013, 1: 1561-1572.

- [11] A M Pires, O. A. Serra and M. R. J. Davolos. *Alloys Compd.*, 2004, 374, 181-184.
- [12] K. W. Kramer, D. Biner, G. Frei, H. U. Gudel, M. P. Hehlen, S. R. Luthi, *Chem. Mater.* 2004, 16, 1244-1251.
- 5 [13] R. Valiente, C. Renero-Lecuna, R. Martin-Rodriguez, *Chem. Mater.*, 2011, 23(15):3442-3448.
- [14] T. Hirai and T. Orikoshi. *J. Colloid Interf. Sci.*, 2004, 269: 103-108.
- [15] T. Sh Atabaev, Z. L. Piao, Y.-H. Hwang, H-K Kim, N. H. Hong. *J. Alloy. Compd.*, 2013, 572:113-117.
- 10 [16] J.G. Deng, D. L. Liu, Y. Liu. *J. Funct. Mater. (in Chinese)*, 2012, 43,109-112.
- [17] M. V. D. Vermelho, A. S. Gouveia-Neto and H. T. Amorim, *J. Lumin.*, 2003, 102-103, 755-761.
- [18] S. H. Ri, Z. H. Bai, X. Y. Zhang and L. P. Lu, *J. Chinese Ceramic Soc.*, 2011, 39, 973-977.
- 15 [19] X. X. Luo and W. H. Cao. *Sci China Series B: Chem (in Chinese)*, 2007, 37, 148-155.
- [20] C. L. Lo, J.G. Duh, B. S. Chiou, C. C. Peng, L. Ozawa. *Mater Chem Phys*, 2001, 71:179-189.
- 20 [21] F. Auzel, *Chem. Rev.*, 2004, 104, 139-173.
- [22] M. Pollnau, D. R. Gamelin, S. R. Luthi, H. U. Gudel and M. P. Hehlen, *Phys. Rev. B*, 2000, 61, 3337-3346.
- [23] H. Y. Zhong and W. H. Cao, *J. Funct. Mater. (in Chinese)*, 2009, 40, 896-899.
- 25 [24] X. X. Luo and W. H. Cao, *Science in China (Series B)*, 2007, 37, 148-155.
- [25] R. Valiente, O. S. Wenger and H. U. Gudel, *J. Chem. Phys.* 2002, 116, 5196-5204.
- [26] R. Martin-Rodriguez, S. Fischer, A. Ivaturi, B. Froehlich, K. W. Kramer, J. C. Goldschmidt, B. S. Richards, A. Meijerink and R. Martin-Rodriguez, *Chem. Mater.*, 2013, 25, 1912-1921.
- 30 [27] P. Gerner and H. U. Gudel, *Chem. Phys. Lett.*, 2005, 413, 105-109.
- [28] J. S. Zhang, L. G. Zhang, J. Y. Ren, P. H. Duan, Y. S. Luo and S. Z. Lv, *Chinese J. Lumin.*, 2013, 34(5), 542-546.
- 35 [29] S.Y. Zhang. Beijing: Science Press, 2008.
- [30] Z. H. Bai, S. H. Ri, X. Y. Zhang, L. P. Lu, Q. S. Liu and X. Y. Mi, *Chinese J. Inorg. Chem.*, 2012, 28(4), 674-678

40

45